Direct Tension and Cyclic Testing of JFE SPF Wave Feature

Submitted to:

JFE Engineering Corporation
Yokohama, Japan

By
B. A. Berger
B. P. Wham
T. D. O'Rourke
H. E. Stewart

Cornell University
School of Civil and Environmental Engineering
Cornell University
Hollister Hall
Ithaca, NY 14853
March, 2018

Acknowledgements

The authors wish to recognize the excellent effort of Cornell graduate and undergraduate students that made these experiments successful. Namely, the contributions of Christina Argyrou, Corbin Atkins, Quinton Hubbell, Chalermpat (Pat) Pariya-Ekkasut, Margaret Stack, Mia Stewart, Bill Tang, and Sarah Weinberg are gratefully acknowledged.

TABLE OF CONTENTS

Acknowledgements i
TABLE OF CONTENTS ii
LIST OF FIGURES iii
LIST OF TABLES iv
Section 1 Introduction 1
1.1. Report Organization 1
1.2. JFE Wave Feature 1
Section 2 Tensile Coupon Tests 3
2.1. Introduction 3
2.2. Specimen Selection and Location 3
2.3. Tensile Coupon Testing and Procedure 3
2.4. Stress vs. Strain Data 5
2.4.1. Young's Modulus and Yield Strength 5
2.4.2. Ultimate Tensile Strength and Strain 6
2.4.3. Poisson's Ratio 8
2.5. Comparison of Test Results to JIS G3101, 2015 SS400 9
Section 3 Straight Pipe and SPF Wave Tension Testing 11
3.1. Introduction 11
3.2. Instrumentation 11
3.3. Test Sequence: Straight Pipe and SPF Tension 16
3.4. Experimental Results: Straight Pipe Tension (TTS) 16
3.4.1. Axial Displacements 16
3.4.2. Pipe Strains 18
3.5. Experimental Results: SPF Tension (TTW1) 18
3.5.1. Axial Displacements 20
3.5.2. Pipe Strains 21
3.5.3. Post-test Images of Wave Feature 22
3.6. Test Sequence: SPF Cyclic (TTW2) 23
3.7. Experimental Results: SPF Cyclic (TTW2) 24
3.7.1. Displacements 25
3.7.2. Pipe Strains 27
3.7.3. Post-test Images of Wave Feature 29
3.8. Tension Test Comparison 30
3.9. Tension Test Conclusions 33
Section 4 Summary 34
4.1. Tensile Coupon Tests 34
4.2. SPF Tension Test 34

4.3. Significance of Test Results 35
References 37

LIST OF FIGURES

Title		Page
Figure 1.1.	SPF wave feature geometry (JFE, Sep. 15, 2015 communication)	2
Figure 2.1.	Schematic of tensile coupon specimen (ASTM – E8 2013)	4
Figure 2.2.	Size comparison of wall cut coupon specimens	4
Figure 2.3.	Baldwin testing apparatus	5
Figure 2.4.	Stress – strain curve for Specimen 1	7
Figure 2.5.	Stress – strain curve for Specimen 2	7
Figure 2.6.	Average Young's modulus and yield stress	7
Figure 2.7.	Stress - strain curve to failure using laser extensometer data	8
Figure 2.8.	Transverse vs. axial strain in elastic range	9
Figure 3.1.	Straight pipe (a) and pipe with SPF (b) strain gage layout	12
Figure 3.2.	Plan view of axial tension test	13
Figure 3.3.	TTS axial force vs. actuator displacement	17
Figure 3.4.	TTS north end cap failure	17
Figure 3.5.	TTS strain vs. actuator displacement	18
Figure 3.6.	TTW1 SPF at several tensile deformation levels	19
Figure 3.7.	TTW1 axial force vs. (a) actuator displacement and (b) wave displacement	20
Figure 3.8.	TTW1 strain vs. (a) actuator displacement and (b) wave displacement	21
Figure 3.9.	TTW1 axial force vs. displacement from strain gages	22
Figure 3.10.	Post-test photos of TTW1 SPF wave feature	23
Figure 3.11.	TTW2 (a) actuator displacement and (b) axial force vs. time	24
Figure 3.12.	TTW2 images of SPF during cyclic motion	26
Figure 3.13.	TTW2 axial force vs. (a) actuator displacement and (b) wave displacement	27
Figure 3.14.	TTW2 axial strain vs. (a) actuator displacement and (b) wave displacement for the duration of test	28
Figure 3.15.	TTW2 axial strain vs. (a) actuator displacement and (b) wave displacement for the cyclic portion of test sequence	28
Figure 3.16.	TTW2 axial force vs. actuator displacement from strain gages	29
Figure 3.17.	Post-test photos of TTW2 SPF wave feature	30
Figure 3.18.	Axial force vs. actuator displacement for (a) full range and (b) first 6 in. (150mm)	32
Figure 3.19.	Actuator force vs. wave displacement for (a) full range and (b) first 2 in. (50mm)	32

LIST OF TABLES

Title		Page
Table 1.1.	Geometric and material properties of JFE SPF test specimen	2
Table 2.1.	Young's modulus and yield stress	6
Table 2.2.	Summary of ultimate tensile stress and strain	8
Table 2.3.	Poisson's ratio measured in elastic range	9
Table 2.4.	Comparison of JFE pipe and hot rolled steel plate material properties	10
Table 3.1.	Instrumentation common to JFE SPF and straight pipe tension test	14
Table 3.2.	Instrumentation for JFE straight pipe tension test	14
Table 3.3.	Instrumentation for JFE SPF tension and cyclic tests	15

Section 1
Introduction

This report is submitted to the JFE Engineering Corporation (herein referred to as JFE). It presents test results from a program to investigate the performance of 8.5-in. (216-mm)-diameter steel pipe with a JFE wave feature for Steel Pipe Crossing Faults (SPF). The purpose of the testing is to evaluate the ability of the SPF to accommodate axial tension and cyclic movement. This is a continuation of previous testing conducted at Cornell to investigate the efficacy of the SPF during fault rupture (Wham et al., 2016). The work was undertaken in the Cornell Large Scale Lifelines Testing Facility, which is part of the Bovay Laboratory Complex at Cornell University.

1.1. Report Organization

The report is organized into four sections. Section 1 provides introductory remarks. Section 2 presents the results of tensile coupon tests performed on steel specimens cut from the wall of a JFE pipe. Section 3 provides the results of direct axial tension and cyclic loading tests. Section 4 summarizes key findings from the preceding sections and provides general conclusions derived from the testing program.

1.2. JFE Wave Feature

Tests were performed on pipe specimens with a geometric inclusion developed by JFE and is referred to in this report as a “wave feature”. All testing was performed on wave features of consistent geometry. A schematic of the wave is presented in Figure 1.1. The wave feature is joined to lengths of straight pipe by circular, full penetration butt welds.

The wave features were manufactured in Japan and shipped to Cornell by JFE. The specimens represent approximate one quarter scale models of a 34 in. (850 mm) diameter pipeline, the smallest typical pipeline diameter for which the wave feature is designed. The pipe and wave feature were constructed of hot rolled steel plate conforming to the JIS SS400 Standard (JIS G3101, 2015). Table 1.1 lists the geometric and material properties of the pipe information provided by JFE.

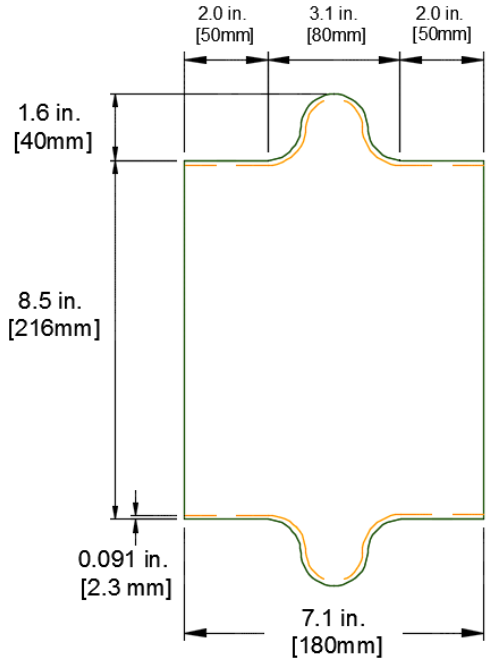

Figure 1.1. SPF wave feature geometry (JFE, Sep. 15, 2015 communication)

Table 1.1. Geometric and material properties of JFE SPF test specimen

Outside Diameter, D	8.5 in. (216 mm)
Wall Thickness, t	0.091 in. (2.3 mm)
Tensile Strength	58 – 74 ksi (400 – 510 MPa)
Yield Strength	44 – 46 ksi (300 – 317 MPa)
Young's Modulus	28.5 – 31.6 x 10^6 ksi (196 – 218 GPa)
Poisson's Ratio	0.27 – 0.29

Section 2
Tensile Coupon Tests

2.1. Introduction

This section describes the uniaxial tensile coupon testing and results. Tensile coupons were machined from an untested pipe wall and tested in tension to evaluate the strength, stiffness, and ductility of the material, and assess if the cold rolling and longitudinal seam welding process results in changes of material behavior. Testing procedures were adapted from ASTM – E8 2013 (ASTM, 2013), and the results are compared to the minimum specifications provided in the JIS SS400 Standard (JIS G3101, 2015) as well as tensile coupon testing performed at Cornell University on JFE hot rolled steel plate.

2.2. Specimen Selection and Location

Three specimens were machined from the pipe wall with a neck thickness (Figure 2.1., dimension 'W') of 0.5 in. (12.5mm). The results of these tests did not agree with typical values of steel or previous tensile coupon test results for JFE steel tested at Cornell (Wham et al., 2016). The results are related to the complex unfolding that occurred as the curved test specimen coupons were stretched and flattened during application of tensile forces on the specimens.

New specimens were obtained from two locations around the circumference of the pipe. They were both approximately 180 degrees from the longitudinal weld, which runs the length of the pipe.

2.3. Tensile Coupon Testing and Procedure

Due to the thin wall and curvature of the specimens, ASTM - E8 2013 (ASTM 2013) could not be followed. The nominal dimensions of the ASTM standard tensile coupons are shown in Figure 2.1. Dimensions C and W were reduced to 0.4 in. and 0.15 in (10.2mm and 3.81mm), respectively. The ASTM standard does not identify a specific wall thickness. Each coupon had a nominal thickness, t, of 0.091 in. (2.3 mm), the thickness of the pipe wall. A comparison of size for specimens described in this section relative to those complying with the ASTM standard is provided in Figure 2.2.

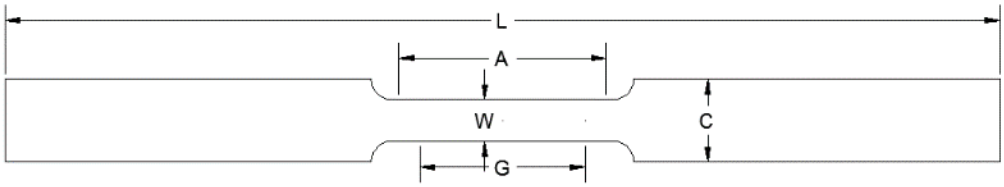

Sheet-Type, .5 in Wide	
Dimensions	*Length (in.)*
G - Gauge Length	2.00
W - Width	0.50
T - Thickness	
R - Radius	0.50
L - Overall Length	8.00
A - Length of Reduced Section	2.25
C - Width of Grip Section	1.00

Figure 2.1. Schematic of tensile coupon specimen (ASTM – E8 2013)

Figure 2.2. Size comparison of wall cut coupon specimens

A Baldwin Hamilton 60 BTE Universal Testing Machine was used to apply tensile loads. The load frame was fitted with a pressure sensor to measure applied force. The machine was calibrated in March of 2017. A photo of the test setup is provided in Figure 2.3.

Two tensile coupon specimens were tested. The specimens were instrumented with axial and transverse strain gages. Bondable axial and transverse strain gages were used to evaluate the stress vs. strain relationship at lower strains because they are considerably more accurate at these levels than other instruments. The gages were adhered to the center of the reduced area of the specimen on the inner and outer wall. This method allows for a correction to bending induced by unfolding. Such gages typically debond at strains of 2 to 4%, rendering them ineffective at larger strain levels.

Figure 2.3. Baldwin testing apparatus

An MTS model LX-500 laser extensometer was used to measure axial strain to failure. This device is not as accurate as the strain gages at smaller strains, but provides for a reliable assessment of strain at larger values, specifically those beyond the initiation of plastic deformation.

2.4. Stress vs. Strain Data

The stress applied throughout the uniaxial tension test was computed by dividing the measured force by the original cross-sectional area of the tensile coupon. The measured strain generally is referred to as engineering strain. The uniaxial stress vs. axial strain plots for each of the three specimens are shown in Figures 2.4 and Figure 2.5. These plots show both the bondable strain gage and laser extensometer data.

An expanded view of the stress vs. strain data is shown in Figure 2.6, in which the combined strain gage and laser extensometer data were used to plot stress vs. strain within and beyond the elastic range. At the end of the elastic range, locally variable readings were obtained with the bondable gages, and preference beyond this range was given to the laser extensometer data in developing the stress vs. strain relationship.

2.4.1. Young's Modulus and Yield Strength

Young's modulus was computed using the elastic range of the stress vs. strain curve and a combination of the bonded axial strain gage and extensometer data. These data are shown to a

strain of 0.0045 in Figure 2.6. Young's Modulus was determined by performing a linear regression for stress vs. strain from 5 ksi to 35 ksi (34 to 241 MPa). The yield strength, σ_y, was computed using the offset method, in which a line parallel to the linear part of the stress vs. strain plot is projected from 0.2% strain. The intersection of this line and the stress vs. strain curve provides an estimate of the yield stress for each specimen. The Young's modulus and yield stress for the specimens are presented in Table 2.1. The average Young's Modulus is 33,200 ksi (229 GPa). The average yield stress is 48.3 ksi (333 MPa).

Table 2.1. Young's modulus and yield stress

Specimen	Young's Modulus, E ksi (GPa)	Offset Yield, σ_y ksi (MPa)
1	32,400 (223)	47.1 (325)
2	33,900 (234)	49.4 (341)
Average	33,200 (229)	48.3 (333)

2.4.2. Ultimate Tensile Strength and Strain

Axial stress vs. strain data from the clip-on extensometers were used to determine the ultimate strength and strain, as shown in Figure 2.7. Table 2.2 gives the failure tensile stress and failure strain for the specimens. The average ultimate stress was 72.7 ksi (501 MPa). The average ultimate strain was 30.7%.

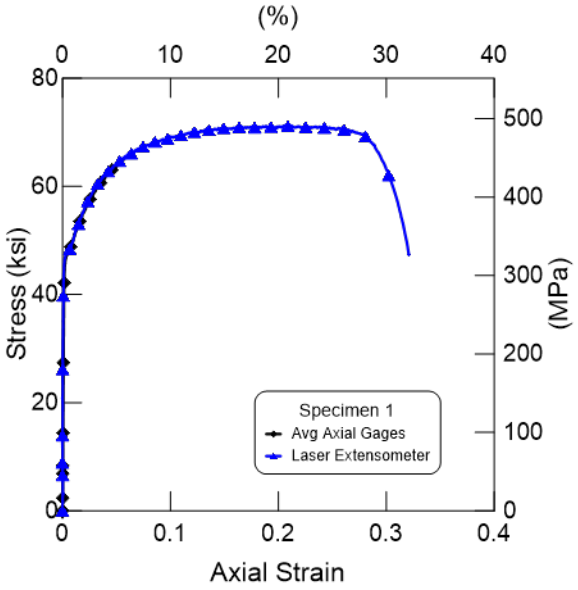

Figure 2.4. Stress – strain curve for Specimen 1

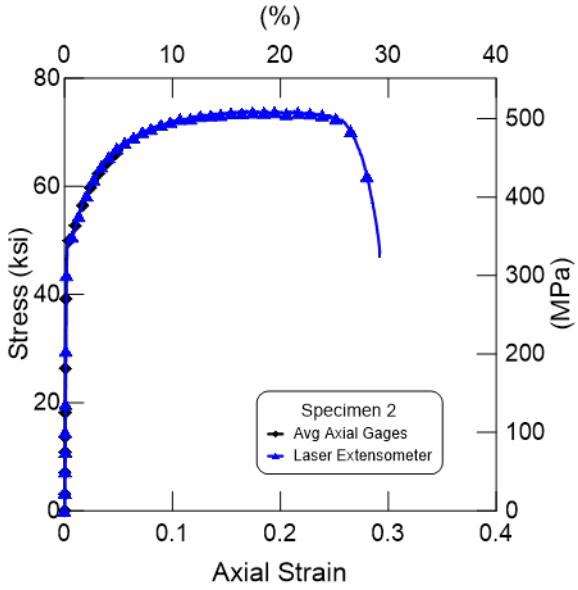

Figure 2.5. Stress – strain curve for Specimen 2

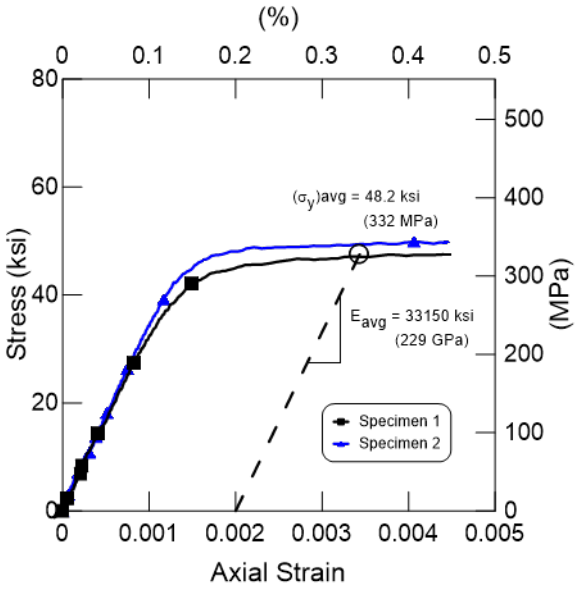

Figure 2.6. Average Young's modulus and yield stress

Table 2.2. Summary of ultimate tensile stress and strain

Specimen	Ultimate Strength, ksi (MPa)	Strain (%)
1	71.3 (492)	32.1
2	74 (510)	29.2
Average	72.7 (501)	30.7

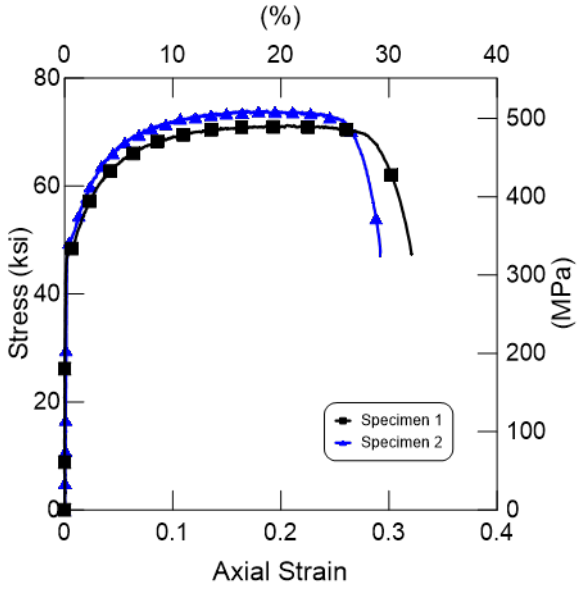

Figure 2.7. Stress - strain curve to failure using laser extensometer data

2.4.3. Poisson's Ratio

Poisson's ratio, ν, is the negative ratio of transverse strain to axial strain for uniaxial loading. Poisson's ratio was derived from the transverse and axial strain gage data for stresses in the elastic range, as shown in Figure 2.8. Poisson's ratio data are presented in Table 2.3. Poisson's ratio for all specimens was 0.27. The Poisson's ratio of 0.27 compares well with the average Poisson's ratio of 0.29 measured for JFE plate steel (Wham et al., 2016).

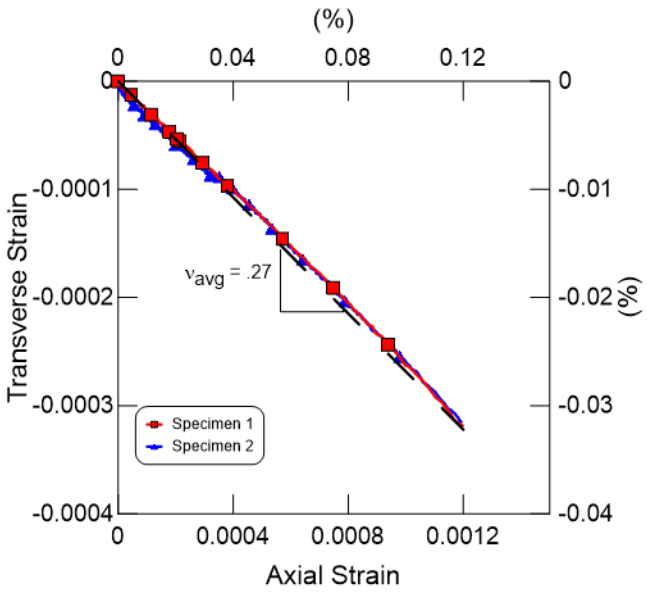

Figure 2.8. Transverse vs. axial strain in elastic range

Table 2.3. Poisson's ratio measured in elastic range

Specimen	Poisson's Ratio, ν
1	0.27
2	0.27
Average	0.27

2.5. Comparison of Test Results to JIS G3101, 2015 SS400

The yield stress, ultimate stress, Young's modulus, and Poisson's ratio are summarized in Table 2.4 and compared with the testing performed on JFE hot rolled plate as well as minimum specifications in the JIS SS400 Standard (JIS G3101, 2015). The yield and ultimate stresses are 27% and 28% greater than the minimum specifications, respectively.

Table 2.4. Comparison of JFE pipe and hot rolled steel plate material properties

Parameter	JFE Wall Cut	JFE Steel Plate	JIS G3101 SS400	Difference Wall Cut-Steel Plate (%)	Difference Wall Cut- JIS G3101(%)
Yield Stress, ksi (MPa)	48.3 (333)	44.8 (309)	35.5 (245)	7	27
Ultimate Stress, ksi (MPa)	74 (510)	65.5 (452)	58-74 (400-510)	11	0-28
Young's Modulus, ksi (GPa)	33,200 (229)	31,500 (217)	-	5	-
Poisson's Ratio	0.27	0.29	-	7	-

Section 3
Straight Pipe and SPF Wave Tension Testing

3.1. Introduction

This section summarizes the results of tension and cyclic testing on pipe with the SPF wave feature. Tension tests were carried out on straight pipe and pipe fabricated with an SPF. A cyclic test was designed to determine if the performance of the SPF diminishes while undergoing cyclic loading. These tests demonstrate wave performance under various loading and pressure conditions that water pipelines might experience during earthquake-induced ground deformation.

The cyclic test was designed to determine if tensile performance of the SPF degrades after compressive displacement is followed by cyclic motion. Based on their finite element modeling, JFE recommended an initial displacement of 1.57 in. (40 mm) in compression. Plus/minus 1.18 in. (30 mm) was used for cyclic motion as a reasonable upper bound for the effects of near field seismic velocity pulses. This test also provides validation for design limits set forth by JFE.

The wave feature, as described in Section 1.2, was joined to lengths of straight pipe sections by welds. As shown in Figure 3.1, the straight sections of pipe were 56.5 in. (1435 mm) long. Flanges were welded to each end of the straight pipe sections to which steel end caps with rubber gaskets were bolted. The flange and end caps allowed for pressurization of the specimen and provided a stiff connection for transferring axial force to the specimen.

3.2. Instrumentation

Figure 3.2 shows a plan view of the tension test setup and key instrumentation. An actuator and load cell were installed at the south end of the load frame to apply and measure force. The Atlas servo-controlled actuator is capable of applying 200 kips (890 kN) in tension and 400 kips (1780 kN) in compression. Four load cells were used at the north end of the pipe to provide redundant axial force measurements. An electronic pressure transducer, located at the north end cap, measured internal water pressure during the test sequence.

Axial pipe movement was measured by three string potentiometers (string pots): N2N, N2S, and Actuator Disp. These string pots are shown in Figure 3.2. String pot, N2N, was positioned between the northernmost side of the load frame and measured relative movement between the north end

of the pipe and the load frame. String pot, N2S, was positioned between the south edge of the northern load beams and the southern end cap of the pipe to measure axial elongation of the test specimen. String pot “Actuator Disp.” was fixed directly to the actuator to measure piston movement. For the tests on pipes with SPF wave features, four string pots were used to measure displacements across the wave feature.

The straight pipe and pipes with SPF wave features had three and four planes of strain gages, respectively, bonded to the pipe. For the straight pipe, gage planes were located at one, two, 3.5, and seven diameters from the southern welded end flange. Gage type and location are summarized in Figure 3.1 and Table 3.2. For the tests on pipes with SPF wave features, a total of 20 strain gages were fixed to the exterior of the specimen at three planes, designated as -30, 0, and +30, as shown in Figure 3.1(b) and Figure 3.2. At each plane the gages were located at the 12, 3, 6, and 9 o´clock positons (crown, east springline, invert, and west springline, respectively). Gage plane -30 was positioned 30 in. (760 mm) south of the wave feature and included four gages oriented in the axial and circumferential directions. Plane +30 was 30 in. (760 mm) north of the wave feature and had four axial gages. Plane 0 was centered on the wave and included four axial and four circumferential gages. The instrument locations and gage names are listed in Table 3.3.

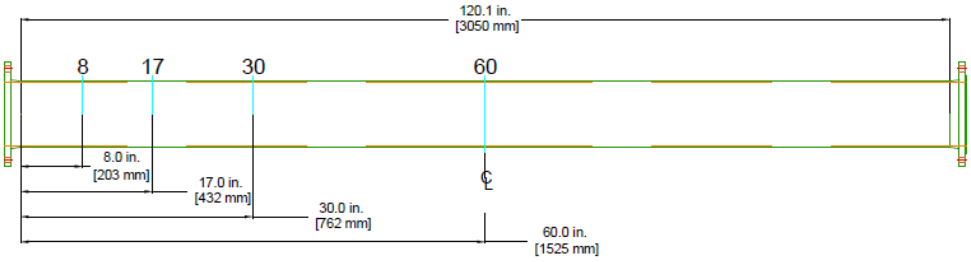

(a)

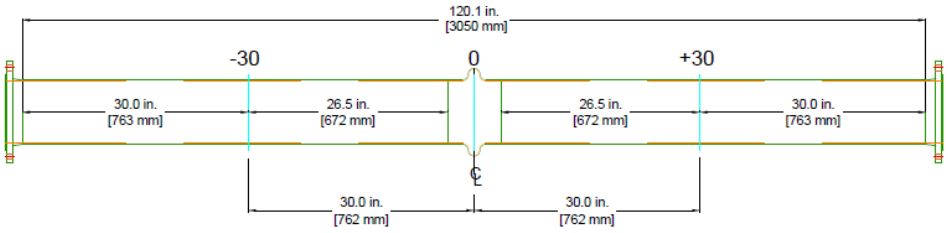

(b)

Figure 3.1. Straight pipe (a) and pipe with SPF (b) strain gage layout

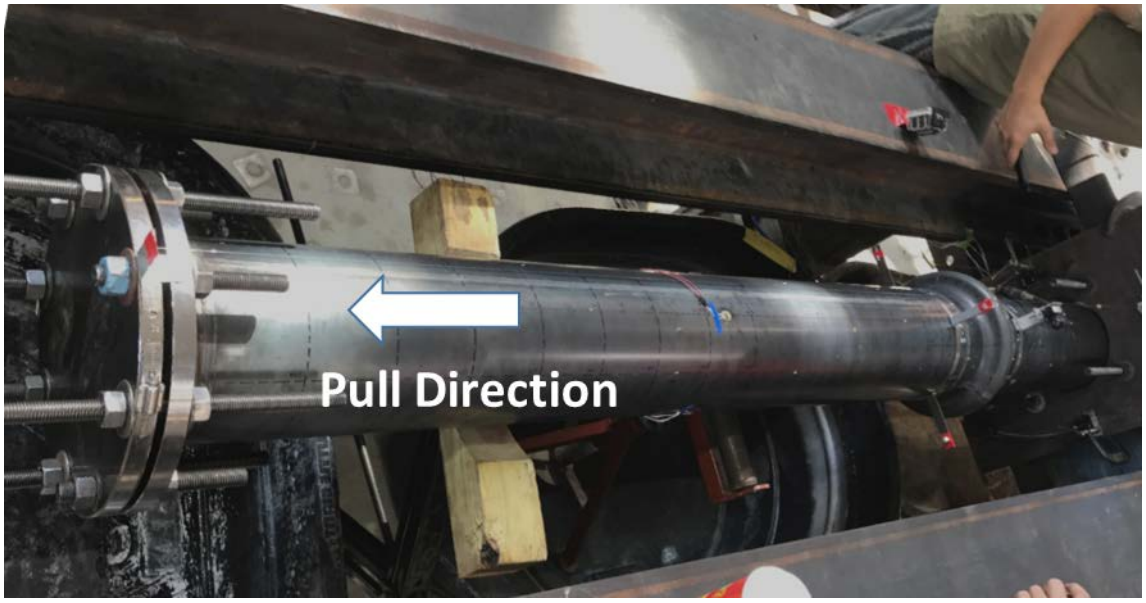

(a)

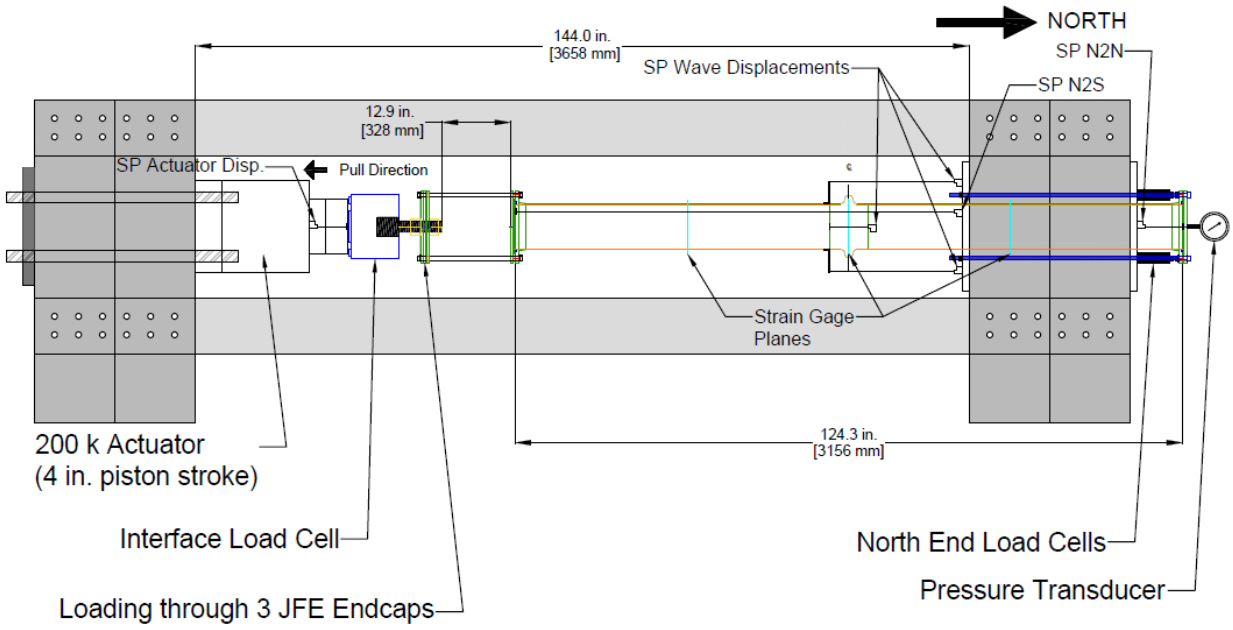

(b)

Figure 3.2. Plan view of axial tension test

Table 3.1. Instrumentation common to JFE SPF and straight pipe tension test

Location	Instrument	Instrument Name
Actuator	String Potentiometer	Act Disp.
Actuator	Interface 400 kip Load Cell	Load
Internal Pressure	Pressure Transducer	Pressure
North End	Load Cell	Top East
North End	Load Cell	Top West
North End	Load Cell	Bottom East
North End	Load Cell	Bottom West
North Edge of North Channel Flange	String Potentiometer	N2N
South Edge of North Channel Flange	String Potentiometer	N2S

1 in. = 25.4 mm

Table 3.2. Instrumentation for JFE straight pipe tension test

Location	Instrument	Instrument Name
8 in. North of South Flange Weld	East Springline, Axial Strain	8E
8 in. North of South Flange Weld	East Springline, Circumferential Strain	8EC
8 in. North of South Flange Weld	West Springline, Axial Strain	8W
8 in. North of South Flange Weld	West Springline, Circumferential Strain	8WC
17 in. North of South Flange Weld	East Springline, Axial Strain	17E
17 in. North of South Flange Weld	East Springline, Circumferential Strain	17EC
17 in. North of South Flange Weld	West Springline, Axial Strain	17W
17 in. North of South Flange Weld	West Springline, Circumferential Strain	17WC
30 in. North of South Flange Weld	East Springline, Axial Strain	30E
30 in. North of South Flange Weld	East Springline, Circumferential Strain	30EC
30 in. North of South Flange Weld	West Springline, Axial Strain	30W
30 in. North of South Flange Weld	West Springline, Circumferential Strain	30WC
60 in. North of South Flange Weld	Crown, Axial Strain	60C
60 in. North of South Flange Weld	Invert, Axial Springline	60I
60 in. North of South Flange Weld	East Springline, Axial Strain	60E
60 in. North of South Flange Weld	East Springline, Circumferential Strain	60EC
60 in. North of South Flange Weld	West Springline, Axial Strain	60W
60 in. North of South Flange Weld	West Springline, Circumferential Strain	60WC

1 in. = 25.4 mm

Table 3.3. Instrumentation for JFE SPF tension and cyclic tests

Location	Instrument	Instrument Name
North Side of SPF	String Potentiometer, Crown	Wave Crown
North Side of SPF	String Potentiometer, Invert	Wave Invert
North Side of SPF	String Potentiometer, East	Wave East
North Side of SPF	String Potentiometer, West	Wave West
30 in. South of CL of SPF	Crown, Axial Strain	-30C
30 in. South of CL of SPF	Crown, Circumferential Strain	-30CC
30 in. South of CL of SPF	Invert, Axial Strain	-30I
30 in. South of CL of SPF	Invert, Circumferential Strain	-30IC
30 in. South of CL of SPF	East Springline, Axial Strain	-30E
30 in. South of CL of SPF	East Springline, Circumferential Strain	-30EC
30 in. South of CL of SPF	West Springline, Axial Strain	-30W
30 in. South of CL of SPF	West Springline, Circumferential Strain	-30WC
CL of SPF	Crown, Axial Strain	0C
CL of SPF	Crown, Circumferential Strain	0CC
CL of SPF	Invert, Axial Strain	0I
CL of SPF	Invert, Circumferential Strain	0IC
CL of SPF	East Springline, Axial Strain	0E
CL of SPF	East Springline, Circumferential Strain	0EC
CL of SPF	West Springline, Axial Strain	0W
CL of SPF	West Springline, Circumferential Strain	0WC
30 in. North of CL of SPF	Crown, Axial Strain	+30C
30 in. North of CL of SPF	Invert, Axial Strain	+30I
30 in. North of CL of SPF	East Springline, Axial Strain	+30E
30 in. North of CL of SPF	West Springline, Axial Strain	+30W

1 in. = 25.4 mm

3.3. Test Sequence: Straight Pipe and SPF Tension

After the specimen was instrumented and centered in the test frame the test sequence was initiated by starting the data acquisition system and laboratory hydraulic systems. The data sampling rate was 2 Hz. The north end load cells, mounted on rods, were slowly tightened. They were adjusted to about 1 kip (4.45 kN) each, totaling 4 kips (17.8 kN) of force. No force was transmitted to the specimen since the south end was free to move. Then the nuts on the south end, where the pipe flange connects to the actuator with 0.75-in. (19-mm) high strength threaded rods, were tightened. These adjustments ensured concentric initial loading conditions and restrained the pipe from axial movement due to internal pressure. Approximately 80 psi (550 kPa) of internal water pressure was applied. The measuring systems were checked and an initial actuator displacement of 3.6 in. (91 mm) was applied.

The actuator used for this test has a stroke of 4 in. (100 mm). Following the initial displacement step, the specimen was unloaded and the actuator was extended. The loading rods connecting the actuator to the south end flange were repositioned to apply a second loading increment. A total axial displacement of 4.4 in. (112 mm) and 5.4 in. (137 mm) was applied for the straight pipe and SPF respectively.

3.4. Experimental Results: Straight Pipe Tension (TTS)

This section covers data collected from the tension test conducted on a 120 in. (3050mm) straight pipe manufactured by JFE. Pressure was maintained at 80 psi (550kPa) for the duration of the test. The straight pipe tension test is referred to as TTS in this report.

3.4.1. Axial Displacements

Displacements were imposed with a servo-controlled hydraulic actuator at the south end of the loading frame. The actuator was retracted (moved south) 0.26 in. (6.6mm) with a corresponding force of 65 kips (289 kN) to check all instrumentation while still in the linear elastic region. Then the actuator was extended (moved north) 0.16 in (4mm) to reduce the load in the system to 12 kips (53 kN). This load cycle is shown in the figure. Once confirmed that all instrumentation was functioning, the pipe was loaded at a rate of 1 in./min (25.4 mm/min) to a global end displacement of 3.6 in. (91mm). Figure 3.3 shows axial force vs. displacement for this loading sequence. After

this initial step, local yielding of the restraining rods was observed in the north end causing bending of the endcap. These rods were replaced with high strength rods for the next loading step. Global displacements were corrected in the data by use of the N2N string pot measuring north end displacement. The actuator was reset and moved an additional 0.8 in. (20mm). A failure at the north end cap, shown in Figure 3.4, occurred by means of weld fracture. The pipe accommodated a total displacement of 4.4 in. (112 mm) at a maximum force of 135 kips (600 kN).

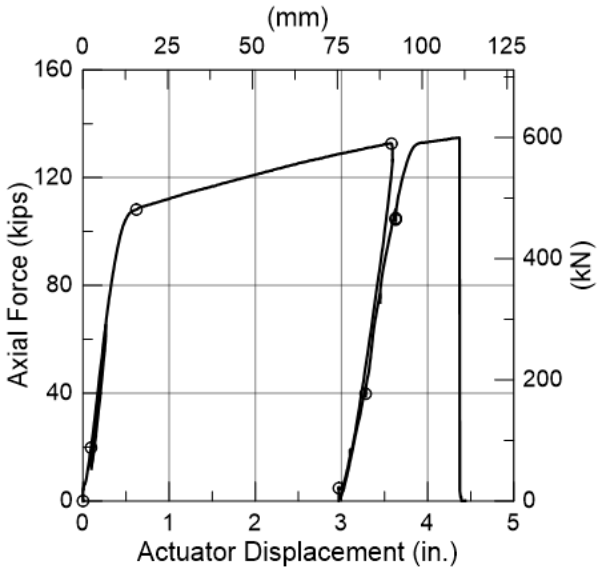

Figure 3.3. TTS axial force vs. actuator displacement

Figure 3.4. TTS north end cap failure

3.4.2. Pipe Strains

Strains were recorded continuously at four planes along the pipe. Planes 8, 17, and 30 consisted of two axial and two circumferential gages. Plane 60 consisted of four axial and two circumferential gages. The averages of each plane are plotted in Figure 3.5. Average axial pipe strain, which is calculated from actuator displacement minus any movement at the restrained end divided by the initial pipe length, is plotted as the dashed line. This overall average strain compares well with strains recorded at the gage planes. During the first unloading step at 3.6 in. (91mm), the strains did not return to zero because of plastic deformation. A small amount of elastic strain on the order of 0.3% was measured after this unloading.

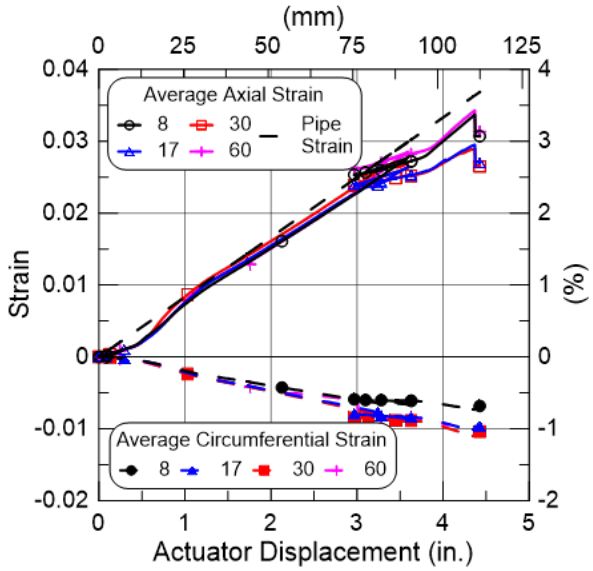

Figure 3.5. TTS strain vs. actuator displacement

3.5. Experimental Results: SPF Tension (TTW1)

This section covers the results of the first tension test on a pipe specimen with an SPF wave feature. For the remainder of the report and all subsequent figures, this test is referred to as TTW1. Figure 3.6 (a)-(f) shows the SPF at approximately 0, 1.0, 2.0, 2.5, 3.0, and 3.5 in. (0, 25, 50, 64, 76, and 89 mm) of actuator imposed deformation, respectively. The pipe failed due to a weld failure at the south flange at a actuator displacement of 5.4 in. (137 mm) and force of 133 kips (592 kN). As the pipe was pulled in tension the wave feature compressed in the circumferential direction, resulting

in reduction of the cross-sectional area of the wave and circumferential buckling. The beginning of buckling is shown in Figure 3.6 (d).

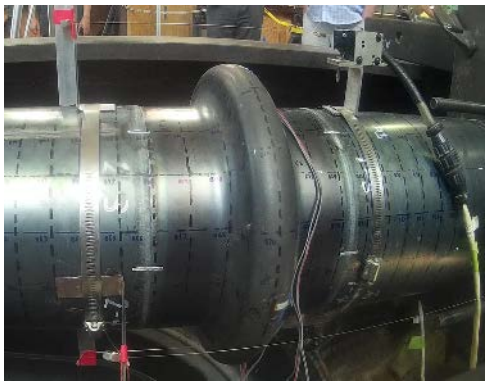

(a) Pre-test

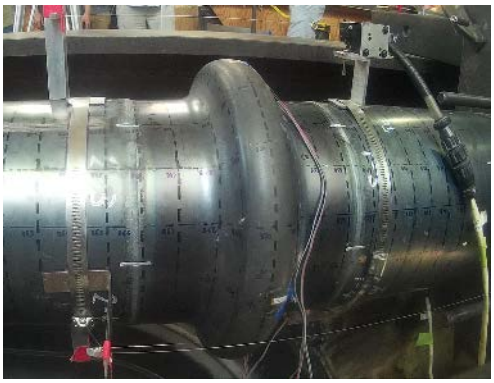

(b) 1 in. (25 mm) axial displacement

(c) 2 in. (50 mm) axial displacement

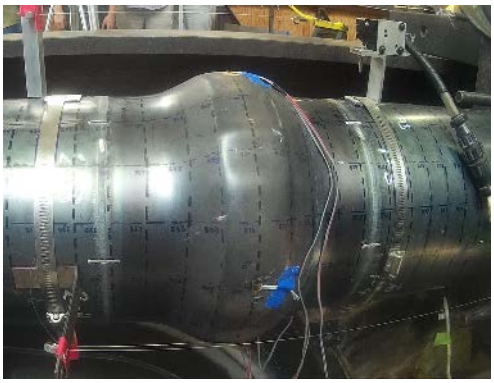

(d) 2.5 in. (64 mm) axial displacement

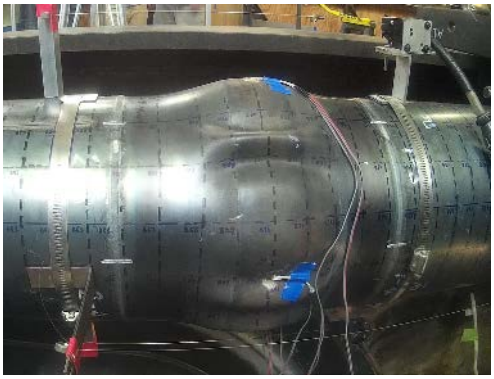

(e) 3 in. (76 mm) axial displacement

(f) 3.5 in. (89 mm) axial displacement

Figure 3.6. TTW1 SPF at several tensile deformation levels

3.5.1. Axial Displacements

Both actuator and wave displacements were recorded. Actuator displacement is calculated using measurements from the string pot mounted on the actuator and subtracting from them relative movements between the pipe and north end of the loading frame measured by the N2N string pot. This displacement is nearly equivalent to the axial elongation of the pipe. Axial wave displacements from weld to weld across the wave feature were measured using string pots at the crown and invert of the pipe. String pot mounts were tightened after each loading step to reduce slippage caused by a reduction in cross-sectional area at the wave.

The initial load increase at zero displacement in Figure 3.7(a) and (b) is due to the application of internal water pressure. The constant tensile load provided by internal water pressure resulted in a small residual axial force after the unloading that followed episode C in Figure 3.7.

There are three distinct regions, A, B, and C, shown in Figure 3.7. A corresponds to opening of the wave feature. B corresponds to the circumferential buckling that occurred as the wave flattened as shown in Figure 3.6 d, e and f. C corresponds post yield and post wave flattening tensile deformation of the pipe. Once the wave flattens, additional strain increments are similar in both the straight pipe and wave feature. The maximum actuator and wave displacements at the end of the test were 5.4 in. (mm) and 2.2 in. (mm), respectively.

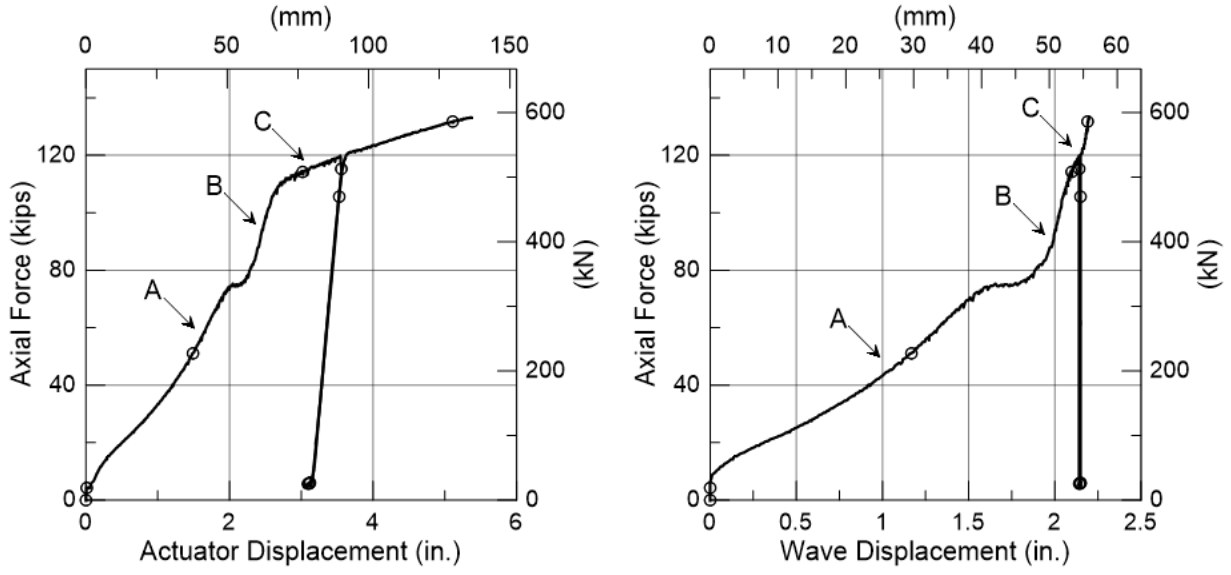

Figure 3.7. TTW1 axial force vs. (a) actuator displacement and (b) wave displacement

3.5.2. Pipe Strains

Pipe strains are reported from two planes of gages, identified as +30 and -30, which were attached to the pipe at plus and minus 30 in. (760 mm) from the centerline of the SPF, respectively. Plane -30 contained axial and circumferential gages at quarter points around the circumference. Plane +30 contained only axial gages at quarter points around the circumference. Figure 3.8 shows average axial and circumferential strains for each location with respect to (a) actuator displacement and (b) wave displacement. The line labeled "Pipe Strain" was calculated by subtracting displacements recorded by the string pots across the wave from the corrected actuator displacement. This is a first-order approximation of average pipe strain, absent the contribution of the wave feature, and it tracks consistently with strains measured by the gages.

The SPF accommodation of axial elongation is demonstrated by its ability to keep the pipe strain low during axial deformation. Through the first 2.5 in. (64 mm) of axial deformation imposed by the actuator, pipe strains remain below 0.5%. It is not until the wave begins to flatten, at approximately 2 in. (50 mm) of wave displacement, that a slope change occurs and strains begin to increase significantly. After the wave flattens strains throughout the wave feature and straight pipe sections increase in a similar manner with the application of additional force.

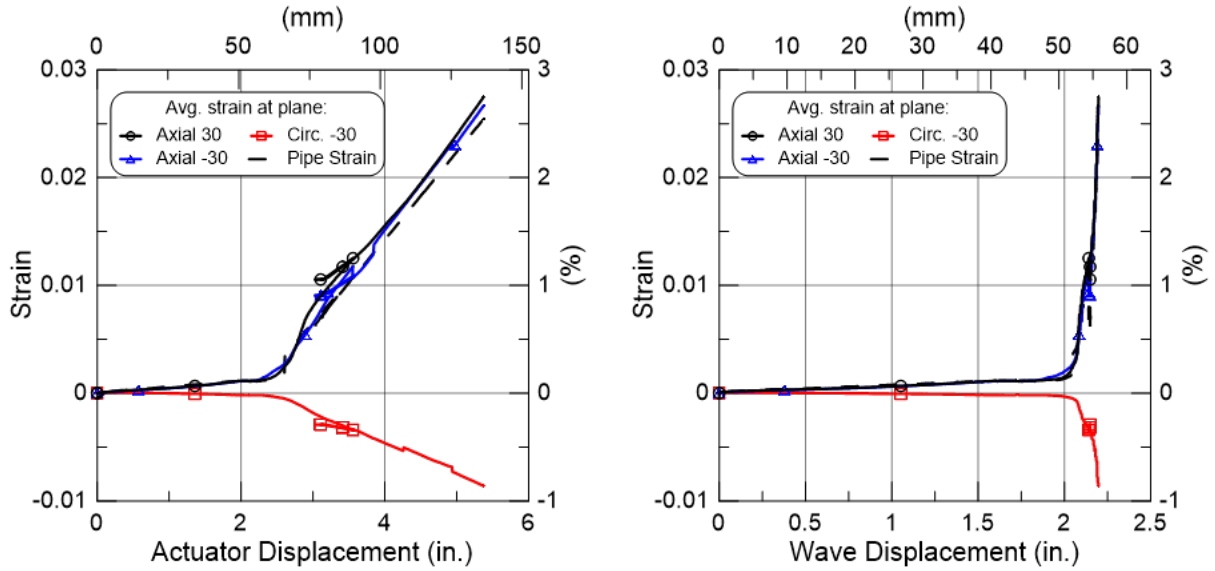

Figure 3.8. TTW1 strain vs. (a) actuator displacement and (b) wave displacement

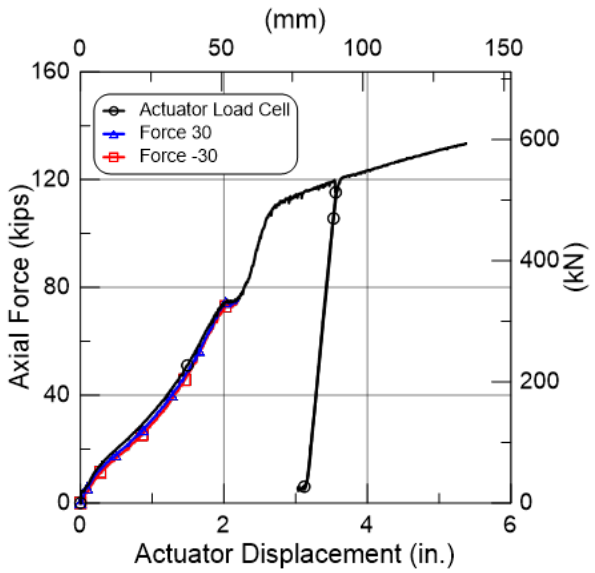

Figure 3.9. TTW1 axial force vs. displacement from strain gages

Using the Young's modulus obtained from tensile coupon tests on pipe wall specimens reported in Section 2, the axial force was evaluated from the strain gages at Planes -30 and +30 during initial expansion of the wave feature. The loads applied at this time, corresponding to episode A in Figure 3.7 are in the elastic range of pipe steel response. Figure 3.9 shows good agreement between the actuator load cell and force calculated from strain.

3.5.3. Post-test Images of Wave Feature

Additional photographs of the SPF wave feature are provided in Figure 3.10. These photographs show the extent of wave elongation and tension field buckling at the crown, springlines, and invert. The images show the full extent of wave deformation under significant loading. Tension field buckling occurs as the larger diameter of the SPF is reduced to a similar diameter as that of the straight pipe sections. Had the cross-section of the wave been perfectly symmetrical, it is expected that a consistent buckling pattern around the circumference of the wave would have been observed. However, the SPF longitudinal weld, as well as local surface imperfections, influence the pattern of buckling. In addition, the welding and rolling processes introduce residual stresses which may influence further the development of buckling.

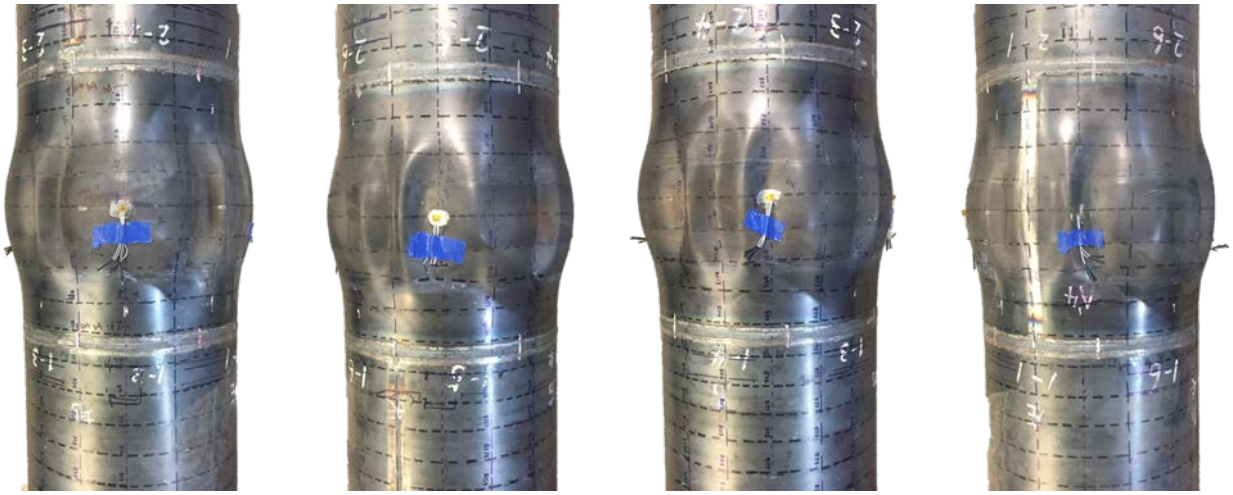

(a) crown (b) invert (c) east springline (d) west springline

Figure 3.10. Post-test photos of TTW1 SPF wave feature

3.6. Test Sequence: SPF Cyclic (TTW2)

After the specimen was instrumented and centered in the test frame the second tension test, TTW2, was initiated by starting the data acquisition system and laboratory hydraulic systems. The data sampling rate was 2 Hz. The north end load cells, mounted on threaded rods, were slowly tightened to about 5 kips (22.25 kN) each, totaling 20 kips (89 kN) of axial force. No force was transmitted to the specimen since the south end was free to move. Since the north load cells can only measure compressive force, preloading provided a means of measuring both applied tensile and compressive axial force during cyclic loading. Next, the nuts were tightened on the south end where the pipe flange and 0.75-in. (19-mm) high strength threaded rods were connected to the actuator. The pipe was filled with water and pressure was maintained between 0 and 10 psi (0-69 kPa) for the entire test. The testing was performed at very low to negligible pressure that provides less resistance to flattening of the SPF wave feature than the 80 psi used in TTW1. The ±2 in. (±50 mm) stroke actuator was positioned at its center of travel, which is identified as 0 displacement. Positive and negative displacements are related to tensile and compressive forces, respectively.

Figure 3.11(a) provides the actuator displacement vs. time for the initial cyclic potion of the test sequence. Episodes A through I in the figure identify each applied displacement increment. Displacement Episode B with 0 in. to -1.57 in. (-40 mm) of actuator displacement was applied at a rate of 1.0 in. (25 mm) per minute to impose compressive displacement consistent with SPF

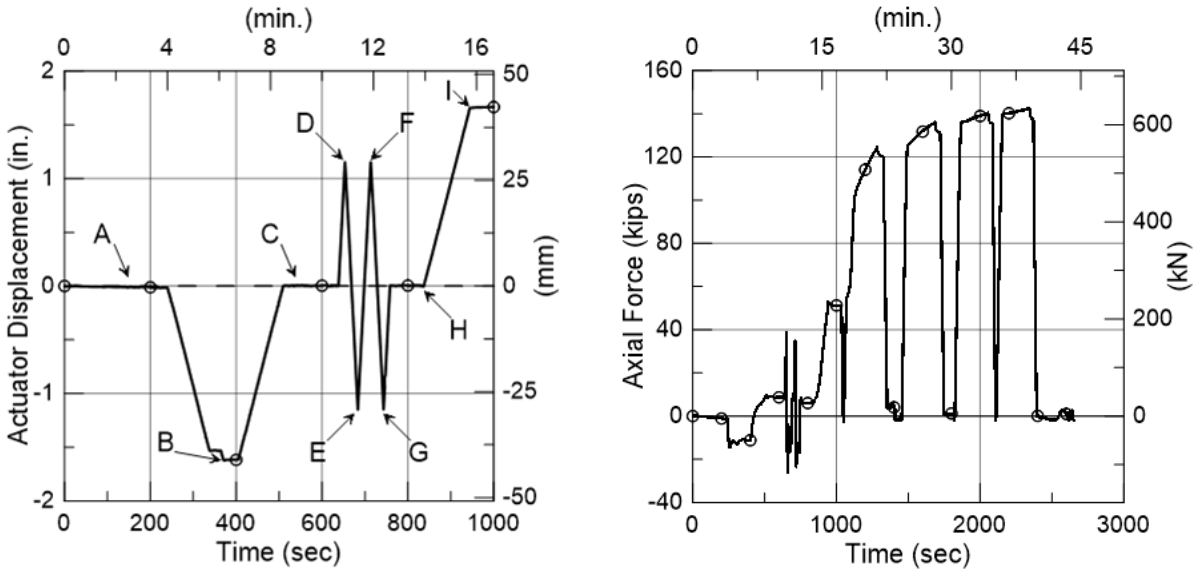

(a) (b)

Figure 3.11. TTW2 (a) actuator displacement and (b) axial force vs. time

deformation capacity. After this step, the actuator was retracted to its initial position of 0 displacement (Episode C). Cyclic motion of ±1.15 in. (30 mm) was imposed on the specimen, starting with positive displacement at a frequency of 0.0167 hz for two cycles (Episodes D through G). Following the two cycles of loading, a subsequent 1.57 in. (63 mm) of tensile displacement was applied to the specimen. This displacement sequence is shown vs. time in Figure 3.11(a). The pipe was then unloaded and disconnected from the actuator. The actuator was fully extended and the end flange was reconnected. A monotonic ramp from -2 in. (-50 mm) to +2 in. (+50 mm) at a rate of 1.0 in. (25 mm) per minute was applied to the specimen. This process of unloading and reloading was repeated after each subsequent pull. The applied load vs. time for the entire test is shown in Figure 3.11(b).

3.7. Experimental Results: SPF Cyclic (TTW2)

This section discusses the results of cyclic testing conducted on the SPF wave feature. A maximum actuator displacement of 14 in. (356 mm) was reached at a force of 142 kips (630 kN). The test was terminated due to space constraints within the load frame. The specimen did not fail, nor was there any indication of leakage detected throughout the entire test sequence.

Figure 3.12(a)–(i) show photographs of the SPF during cyclic motions. Each figure, (a) through (i), corresponds to their respective letters in Figure 3.11 (a). After the first compressive movement, the SPF returned to a geometry configuration nearly identical to its undeformed shape, as shown in Figure 3.12 (a)-(c). The first compressive step of the cyclic displacement [Figure 3.12(e)] induced SPF deformation out of plane with the vertical. Figure 3.12 (g) and (h) show that similar out of plane movement was observed in the second compressive step as well as the return to 0 axial displacement.

3.7.1. Displacements

As in TTW1, both actuator and wave displacement were measured and reported herein. On the first loading step, the wave accommodated 1.5 in. (38 mm) of compressive displacement with a peak force of 14.6 kips (65 kN). The actuator was returned to 0 with a maximum tensile force of 9 kips (40 kN). The wave did not return to its initial position due to some irrecoverable deformation in the loading system. When the actuator was at 0 displacement, measurements indicated a wave compressive displacement of 0.06 in. (1.5 mm). During the first cycle, the peak tensile and compressive loads and displacements were +38 kips (169 kN) at +1.0 in. (25 mm) and -26 kips (116 kN) at -1.0 in. (-25 mm), respectively. The second cycle consisted of peak tensile and compressive loads and displacements of +35 kips (156 kN) at +1.0 in. (25 mm) and -23.6 kips (105 kN) at -1.0 in. (25 mm), respectively. Figure 3.13 (a) and (b) presents axial force vs. actuator and wave displacement, respectively.

Based on the tensile coupon test results reported in Section 2 and cross-sectional pipe area, the axial force necessary to yield the pipe is 98 kips (436 kN). Peak forces experienced during cyclic movement did not exceed 40% of the level to cause yielding of the straight pipe sections. Thus, the pipe barrel remained within its elastic limit during cyclic loading.

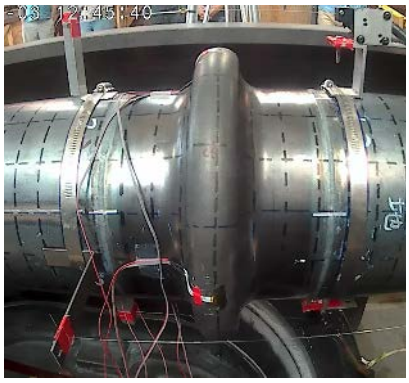

(a) 0 in. axial displacement

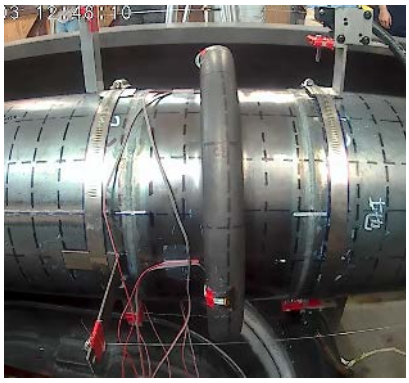

(b) -1.6 in. (41 mm) axial displacement

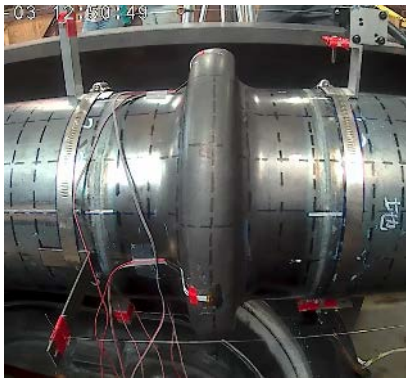

(c) 0 in. axial displacement

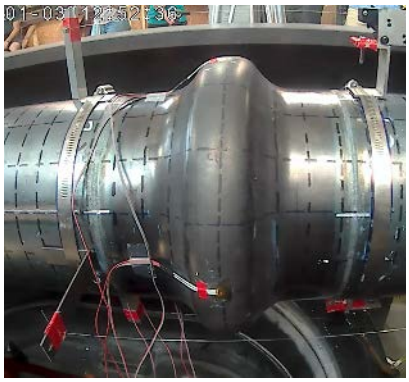

(d) +1.15 in. (30 mm) axial displacement

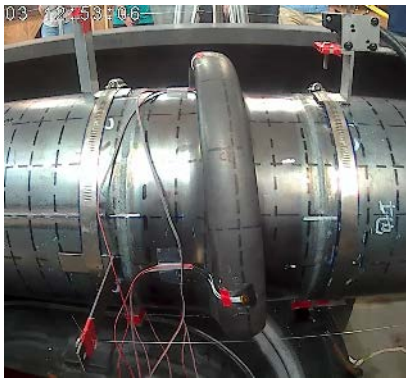

(e) -1.15 in. (-30 mm) axial displacement

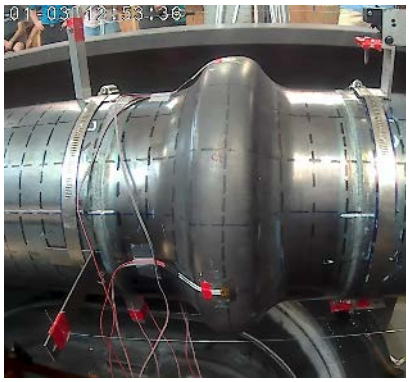

(f) +1.15 in. (+30 mm) axial displacement

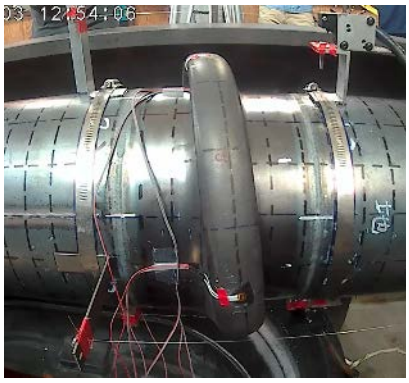

(g) -1.15 in (30 mm) Axial displacement

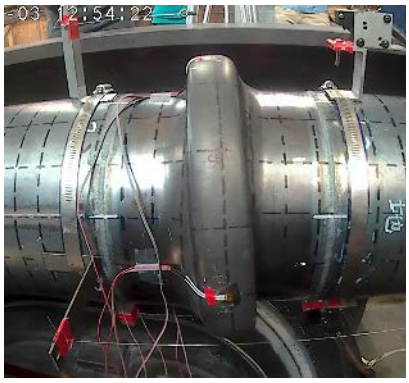

(h) 0 in. Axial Displacement

(i) +1.66 in. (+42 mm) Axial Displacement

Figure 3.12. TTW2 images of SPF during cyclic motion

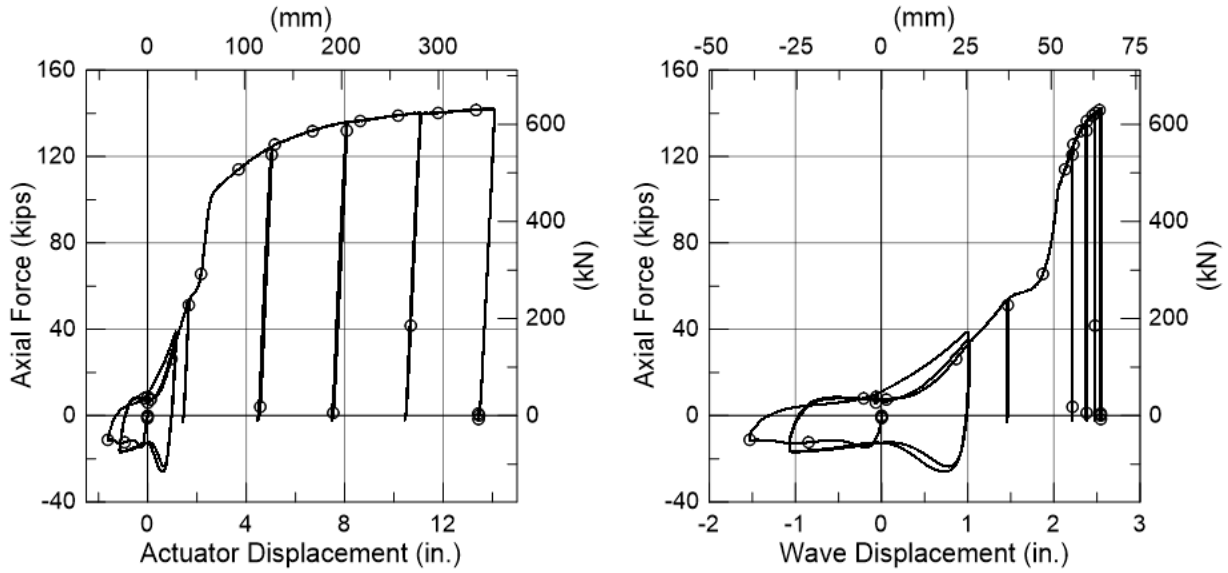

(a) (b)

Figure 3.13. TTW2 axial force vs. (a) actuator displacement and (b) wave displacement

3.7.2. Pipe Strains

Strain gage results are presented for the axial and circumferential strain gages at the +30 and -30 gage planes. Plane -30 consisted of both axial and circumferential gages while plane +30 had only axial gages. Figure 3.14 shows the average axial strains at the north and south gage planes. The figure also shows that the overall average pipe strain, calculated in the same way as for TTW1 in Section 3.5.2, tracks well with the strains measured by the gages. The gages at the +30 plane remained bonded for over 13 in. (330 mm) of actuator displacement and recorded strains above 8.5% before debonding. The -30 plane debonded at 4.1% strain. The circumferential gages recorded a maximum strain of approximately 1.8% before debonding. This strain level was solely induced by axial loading as water pressure was held at or near 0 psi throughout the test.

During cyclic motion, the straight pipe sections experience very low strains relative to the level of axial displacement. This response is a consequence of the SPF wave feature, which absorbs movement while the pipe barrel remains in the elastic range. Figure 3.15 shows that maximum pipe strains are bounded by ±500 με. The strain the SPF accommodates can be calculated from string pot measurements spanning the wave feature. Wave strain, defined as the measured wave expansion (change in weld to weld wavelength minus initial weld to weld length) divided by the

initial weld-to-weld axial wave length, was on the order of ±12% through the initial loading steps, and reached about 25% when the wave feature flattened.

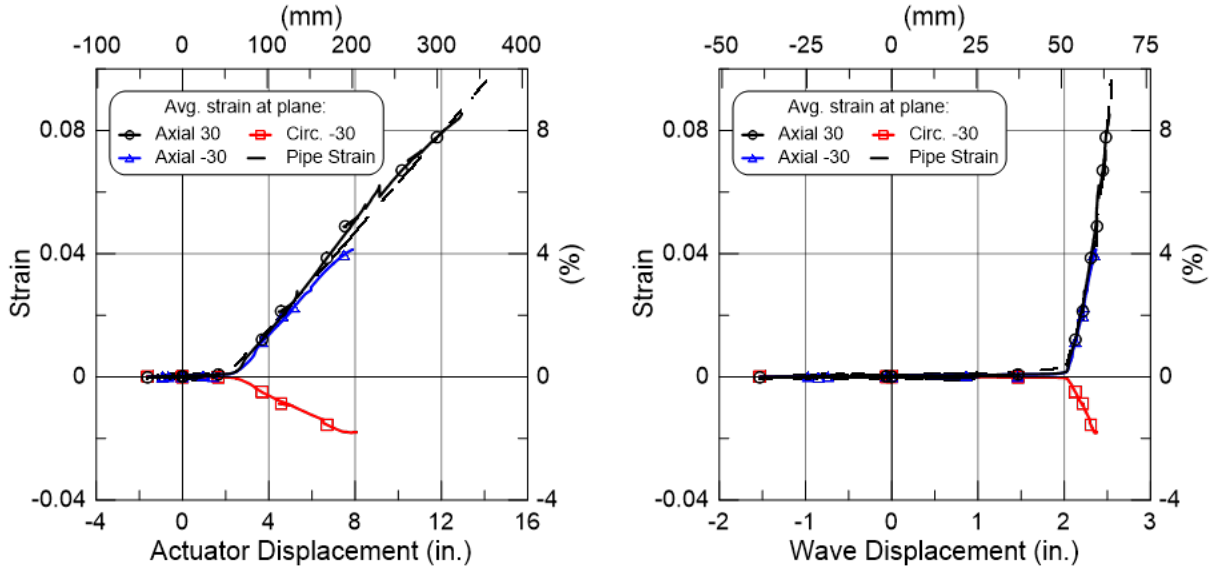

Figure 3.14. TTW2 axial strain vs. (a) actuator displacement and (b) wave displacement for the duration of test

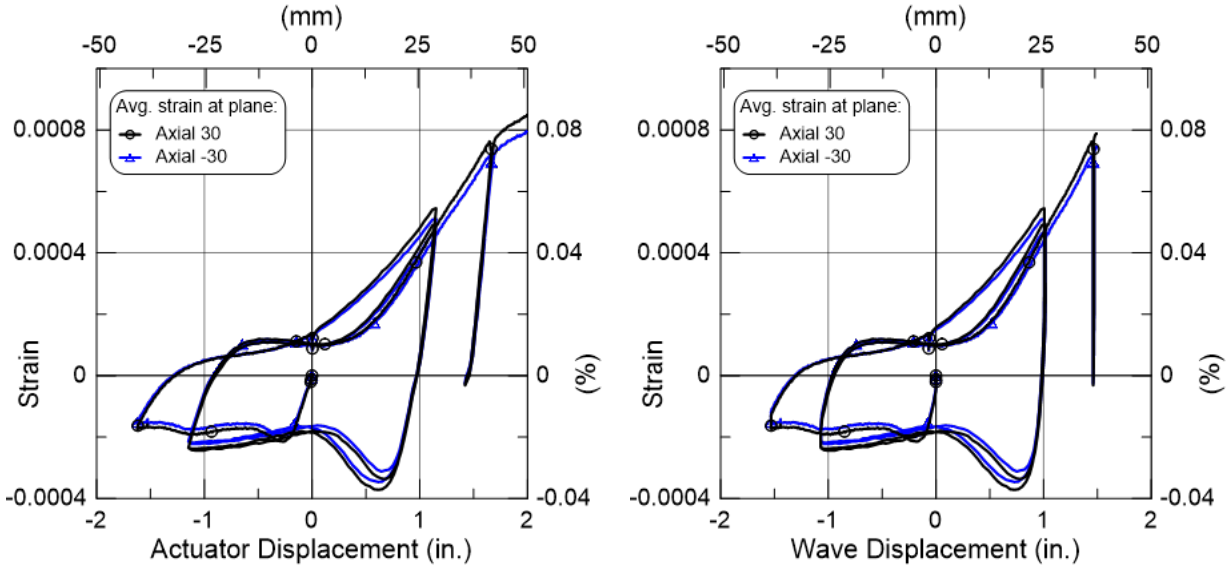

Figure 3.15. TTW2 axial strain vs. (a) actuator displacement and (b) wave displacement for the cyclic portion of test sequence

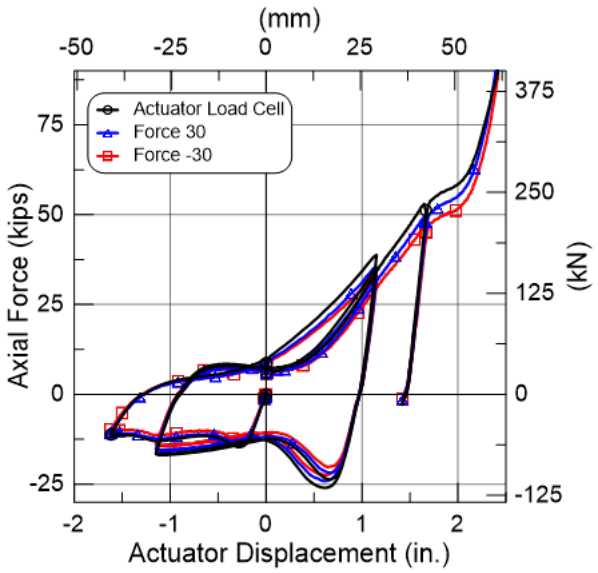

Figure 3.16. TTW2 axial force vs. actuator displacement from strain gages

Using the Young's modulus obtained from tensile coupon tests on pipe wall specimens reported in Section 2, the axial force was evaluated from the strain gages at Planes -30 and +30 during initial loading in TTW2. The loads applied in the initial compression, cyclic deformations, and tensile loading phases are in the elastic range of pipe steel response outside the wave feature. Close agreement between the axial force calculated from gage planes and recorded by the actuator load cell through the first unload reload cycle are shown in Figure 3.16.

3.7.3. Post-test Images of Wave Feature

Additional photographs of the SPF wave feature are provided in Figure 3.17. These photographs show the extent of wave elongation and tension field buckling at the crown, springlines, and invert. The images show the full extent of wave deformation under significant loading.

(e) crown (f) invert (g) east springline (h) west springline

Figure 3.17. Post-test photos of TTW2 SPF wave feature

3.8. Tension Test Comparison

Three tests were performed on JFE pipe, two of which had SPF wave features. The first straight pipe test, TTS, can be considered a baseline for comparison with SPF performance. The second test, TTW1, provides the force-displacement relationship of the SPF in direct tension. The third test, TTW2, provides insight as to how the wave accommodates cyclic motion and if tensile capacity is compromised as a result. The comparison of TTW1 and TTW2 also provides some indication of the influence of internal pressure on wave performance. TTW1 was conducted at 80 psi (550 kPa) of internal water pressure. In contrast, TTW2 was performed with water present, but absent significant internal pressure.

Figure 3.18 (a) shows a comparison of the three tension tests over the full range of displacement. Both TTS and TTW1 experienced failure at their endcaps, at axial displacements well below the pipe extension that can be accommodated in the field. In comparison, TTW2 was deformed without end cap failure well into the plastic strain region of straight pipe response. As stated previously, the test was terminated due to space constraints within the load frame. The specimen did not fail, nor was there any indication of leakage detected throughout the entire test sequence.

Figure 3.18 (b) provides an expanded view of axial force vs. displacement to 6 in. (150 mm) over comparable levels of movement.

The straight pipe yields after 0.5 in. (13mm). At 2 in. (50 mm) of actuator displacement, the straight pipe strains are on the order of 1.5% while both specimens outfitted with an SPF are at strains below 0.13%. Similar slopes of axial force vs. displacement before a yield force of approximately 100 kips (445 kN) are observed in the SPF tests (TTW1 and TTW2). The axial stiffness under tension is substantially less than that of the straight pipe (TTS) for displacement less than about 2.5 in. (63 mm) due to extension of the wave features. Once the SPF wave feature has flattened, the pipe accommodates elastic and plastic strain in a similar manner to the straight pipe. The test results show that the SPF does not hinder tensile performance of the pipe, including deformation well beyond yield for straight pipe sections. This observation of SPF performance holds true even after the SPF is subject to high cyclic deformation representative of the effects of upper bound near field velocity pulses. The SPF wave was shown to accommodate relatively large cyclic movements while allowing the pipe to remain below yield at displacement four times greater than those attained by a straight section of pipe without an SPF wave feature.

Axial force vs. wave displacement plots are shown in Figure 3.19. The plots show some degradation in tensile force required to open the SPF wave feature. An axial force of 43 kips (191 kN) was required to displace the wave 1.0 in. (25 mm) during TTW1. Axial forces of 38 and 34 kips (169 and 151 kN) were required to reach 1.0 in. (25 mm) of wave displacement during cyclic motion followed by 32.5 kips (144 kN) during the next direct tension step.

Degradation of force is not observed on the compression side of cyclic motion. The first monotonic push resulted in an axial force of -13 kips (-58 kN) at a wave displacement of -1.0 in. (-25 mm). The two cyclic motions that followed correspond to an axial force of -16.5 and -16.8 kips (-73.4 and -74.7 kN), respectively.

There is no clear evidence that the presence or absence of internal pressure has a significant effect on the axial force vs. displacement relationship of the SPF. There is close similarity of slopes between the elastic portion of TTW1 plot and the unload/reload slopes of the TTW2 plot. There is a difference in the axial force required to reach the “knee” in the force-displacement relationship, designated as “A” in Figure 3.19 (b), but this difference is more likely associated with the degradation, or loss of stiffness, associated with cyclic loading than with the influence of 80 psi (550 kPa) of internal water pressure.

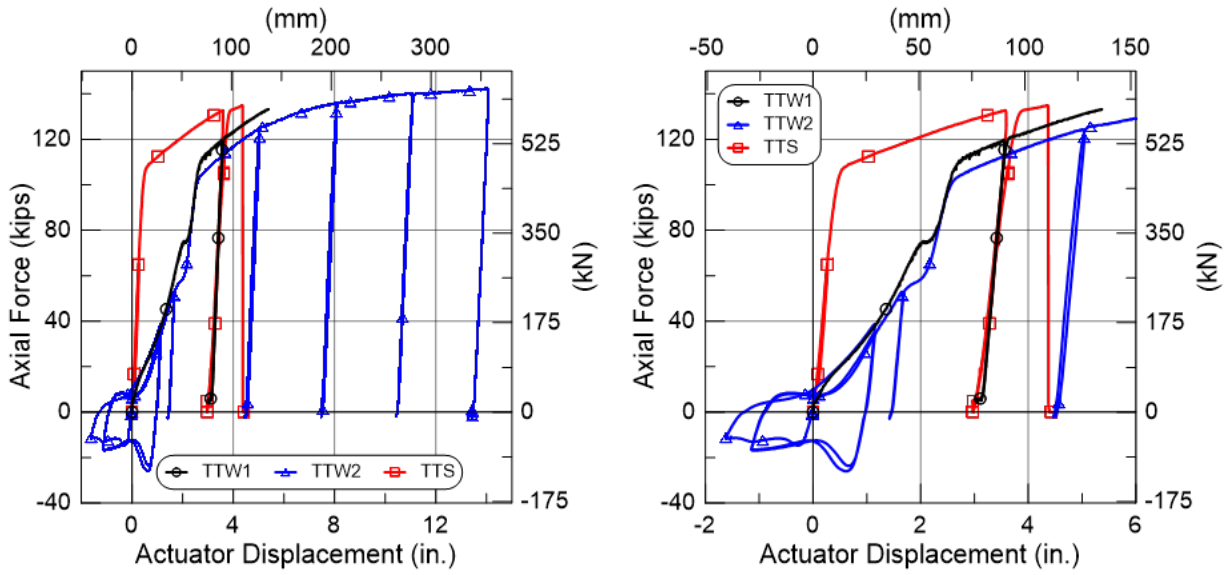

Figure 3.18. Axial force vs. actuator displacement for (a) full range and (b) first 6 in. (150mm)

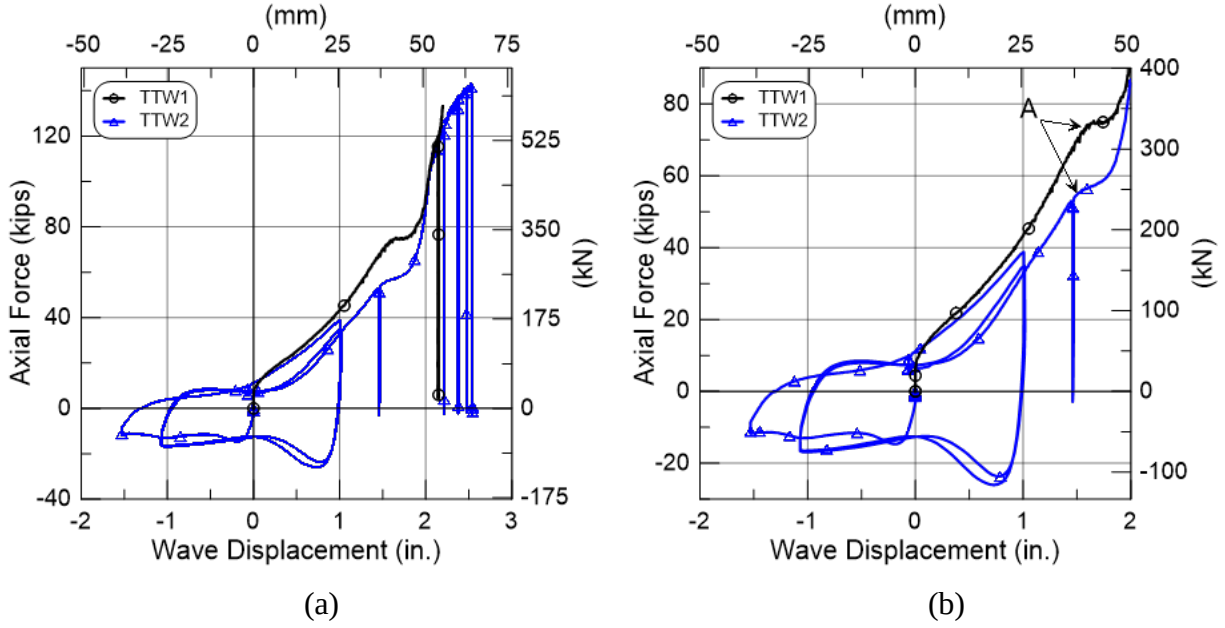

Figure 3.19. Actuator force vs. wave displacement for (a) full range and (b) first 2 in. (50mm)

3.9. Tension Test Conclusions

Three tension tests were performed on 120 in. (3050 mm) sections of SS 400 pipe. Two of these tests, TTW1 and TTW2, had a JFE SPF wave feature included at their midpoint. TTS and TTW1 were pressurized internally to a minimum of 80 psi (550 kPa). TTW2 was conducted with pressure ranging from 0-10 psi (0-69 kPa). The three tests reached axial forces and displacements of 135 kips (600 kN) at 4.4 in. (112 mm), 133 kips (592 kN) at 5.4 in. (137 mm), and 142 kips (630 kN) at 14 in. (356 mm), respectively. Both TTS and TTW1 experienced failure at their endcaps, at axial displacements well below the pipe extension that can be accommodated in the field. TTW2 did not failure or leak, but was stopped after 14 in. (356 mm) of displacement because of space constraints in the loading frame.

The straight pipe experienced yield after approximately 0.5 in. (13 mm) of axial displacement while both pipes outfitted with an SPF wave feature yielded after 2 in. (50 mm) of axial displacement. The SPF wave was shown to accommodate relatively large cyclic movements while allowing the pipe to remain below yield at displacement four times greater than those attained by a straight section of pipe without an SPF wave feature.

Section 4
Summary

This report presents the test results from a program to investigate the performance of an 8.5-in. (216-mm)-diameter steel pipe with a JFE wave feature for Steel Pipe Crossing Faults (SPF). The purpose of the testing is to evaluate the ability of the SPF to accommodate axial tension and cyclic deformation.

4.1. Tensile Coupon Tests

Uniaxial tension testing was performed on the specimens cut from the wall of JFE pipe. Tensile coupons were tested in tension to evaluate the strength, stiffness, and ductility of the material. The average yield stress and ultimate stress determined from the direct tension tests are 48.3 ksi (333 MPa) and 72.7 ksi (501 MPa), respectively. The average Young's modulus was 33,200 ksi (229 GPa), and Poisson's ratio was 0.27. The results of the tensile coupon tests meet the criteria in the JIS SS400 Standard (JIS G3101, 2015).

4.2. SPF Tension Test

Three tension tests were performed on 120-in. (3050-mm)-long test specimens of SS 400 pipe. Two of these tests, TTW1 and TTW2, had a SPF weld feature at the pipe specimen midpoint. TTS and TTW1 were pressurized to a minimum of 80 psi (550 kPa). TTW2 was conducted with pressure ranging from 0-10 psi (0-69 kPa). The three tests reached axial forces and displacements of 135 kips (600 kN) at 4.4 in. (112 mm), 133 kips (592 kN) at 5.4 in. (137 mm), and 142 kips (630 kN) at 14 in. (356 mm), respectively. Both TTS and TTW1 experienced failure at their endcaps, at axial displacements well below the pipe extension that can be accommodated in the field. In comparison, TTW2 was deformed without end cap failure well into the plastic strain region of straight pipe response. The TTW2 test was terminated due to space constraints within the load frame. The specimen did not fail, nor was there any indication of leakage detected throughout the entire test sequence.

The straight pipe experienced yield after approximately 0.5 in. (13 mm) of axial displacement while both pipes outfitted with an SPF wave feature yielded after 2 in. (50 mm) of axial displacement. The SPF wave was shown to accommodate relatively large cyclic movements while

allowing the pipe to remain below yield at displacement four times greater than those attained by a straight section of pipe without an SPF wave feature.

4.3. Significance of Test Results

Previous large-scale fault rupture tests at Cornell demonstrate the ability of the JFE SPF wave features to accommodate significant fault movement through axial compression and deflection of the wave features. The test results reported herein provide a complimentary assessment of SPF wave performance under tension as well as cyclic deformation consistent with upper bound near field velocity pulses. The results demonstrate the ability of the JFE SPF wave features to accommodate substantial tensile deformation through axial displacement of the wave feature as well as tensile strains associated with elongation of the pipe barrel.

Direct scaling of the test results to nominal pipeline diameters in the range of 32 in. (~0.8 m) or more imply that JFE SPF pipelines have the ability to accommodate tensile ground displacements without pipeline rupture or significant loss of water pressure. Comparable performance in the field assumes competent welding and construction practices, consistent with those of the specimens tested, and the absence of significant corrosion or other material imperfections that could compromise pipeline integrity.

The amount of tensile strain that can be accommodated with JFE SPF pipelines will depend on the number and spacing of wave features relative to the location of abrupt ground movement. In test TTW2 the pipe was able to accommodate 14 in. (356 mm) of axial extension, corresponding to an average tensile strain of 11.7% along the 10-ft (3-m) - long pipeline.

Such extension is large enough to accommodate the great majority (over 99%) of liquefaction-induced compressive ground strains measured by high resolution LiDAR after each of four major earthquakes during the recent Canterbury Earthquake Sequence (CES) in Christchurch, NZ (Bouziou, et al., 2015; O'Rourke, et al., 2014). To put the CES ground strains in perspective, liquefaction-induced ground deformation measured in Christchurch exceed those documented in San Francisco during the 1989 Loma Prieta earthquake (e.g., O'Rourke and Pease, 1997; Pease and O'Rourke, 1997) and in the San Fernando Valley during the 1994 Northridge earthquake (e.g., O'Rourke, 1998). They are comparable to the levels of most severe liquefaction-induced ground deformation documented for the 1906 San Francisco earthquake, which caused extensive damage

to the San Francisco water distribution system (e.g., O'Rourke and Pease, 1997; O'Rourke, et al., 2006).

Based on the results of the testing program reported herein, the JFE SPF system performs well under large-scale tensile loading. When the results of the tension testing program are combined with those previously reported for response to compressive ground deformation (Wham et al., 2016), the combined results indicate that JFE SPF system will perform well under most orientations of abrupt ground rupture relative to pipeline alignment, including compressive and tensile ground displacements.

References

ASTM International (2013). “Standard Test Methods for Tension Testing of Metallic Materials”, *ASTM Standards*. E8/E8M - 13a, 1 – 28.

Bouziou, D., T.D. O’Rourke, M. Cubrinovski, and D. Henderson (2015) “Evaluation of Ground Deformations during the 2010-2011 Canterbury Earthquake Sequence”, Proceedings, 6th Intl. Conf. on Earthquake Geotech. Engr., Christchurch, NZ, 8.

Japanese Standards Association, “Rolled Steel for General Structure,” JIS G 3010, 2015 Ed., Aug. 2015.

O’Rourke, T.D. (1998). “An Overview of Geotechnical and Lifeline Earthquake Engineering”, Geotechnical Special Publication No. 75, ASCE, Reston, VA, Proceedings of Geotechnical Earthquake Engineering and Soil Dynamics Conference, Seattle, WA, Aug. 1998, Vol. 2, pp.1392-1426.

O’Rourke, T.D. and J.W. Pease (1997). “Mapping Liquefiable Layer Thickness for Seismic Hazard Assessment”, Journal of Geotechnical Engineering, ASCE, New York, NY, Vol. 123, No.1, January, pp. 46-56.

O’Rourke, T.D., A. Bonneau, J. Pease, P. Shi, and Y. Wang (2006). “Liquefaction Ground Failures in San Francisco”, Earthquake Spectra, EERI, Oakland, CA, Special 1906 San Francisco Earthquake, Vol. 22, No. 52, Apr., pp. 691-6112.

O’Rourke, T.D., Jeon, S-S., Toprak, S., Cubrinovski, M., Hughes, M., van Ballegooy, S., and Bouziou, D. (2014) “Earthquake Response of Underground Pipeline Networks in Christchurch, NZ”, Earthquake Spectra, EERI, Vol. 30, No.1, pp. 183-204.

Pease, J.W. and T.D. O’Rourke (1997), “Seismic Response of Liquefaction Sites”, Journal of Geotechnical Engineering, ASCE, New York, NY, Vol. 123, No. 1, January, pp. 37-45.

Wham, B.P., O’Rourke, T.D. Stewart, H.E., Bond, T.K., & Pariya-Ekkasut, C. (2016). “Large-Scale Testing of JFE Steel Pipe Crossing Faults: Testing of SPF Wave Feature to Resist Fault Rupture,” Cornell University, Ithaca, NY, https://lifelines.cee.cornell.edu/ , last accessed November 16, 2017.